ARTICLE

Size-Dependent Reactivity of Chromium Oxide Cluster Anions $(CrO_3)_{1-4}O^-$ towards Alkanes†

Gong-Ping Wei[a,b,c], Yan-Xia Zhao[a,c*], Sheng-Gui He[a,b,c]

a. State Key Laboratory for Structural Chemistry of Unstable and Stable Species, Institute of Chemistry, Chinese Academy of Sciences, Beijing 100190, China
b. University of Chinese Academy of Sciences, Beijing 100049, China
c. Beijing National Laboratory for Molecular Sciences, CAS Research/Education Center of Excellence in Molecular Sciences, Beijing 100190, China

(Dated: Received on March 30, 2023; Accepted on May 15, 2023)

The reactivity of chromium oxide cluster anions $(CrO_3)_{1-4}O^-$ towards low carbon (C_1-C_4) alkanes has been experimentally investigated at 298 K by employing a homemade ship-lock-type reactor coupled with a time-of-flight mass spectrometer. The results demonstrate that while CrO_4^- and $Cr_2O_7^-$ clusters could abstract a hydrogen atom from C_2H_6 and CH_4, respectively, $Cr_3O_{10}^-$ and $Cr_4O_{13}^-$ clusters were found to be inert towards n-C_4H_{10} within the detection limit. Theoretical results reveal that CrO_4^- and $Cr_2O_7^-$ clusters possess delocalized chromium-bonded oxygen radicals ($Cr-O^{-\cdot}$), which rationalizes the hydrogen atom abstraction reactions between $(CrO_3)_{1,2}O^-$ clusters and alkanes. However, the active sites of $(CrO_3)_{3,4}O^-$ clusters evolve to peroxide species (O_2^{2-}), which exhibit inferior activity compared to $O^{-\cdot}$ radicals. The increase of Cr-3d orbital energy driven by the more negative charge around CrO_y unit formed via downsizing the cluster size has been proposed to account for favorable reduction of O_2^{2-} and selective generation of reactive $O^{-\cdot}$ radicals in small-sized $(CrO_3)_{1,2}O^-$ clusters. This study not only enriches the chemistry of metal-bonded $O^{-\cdot}$ radicals toward alkane activation under mild conditions, but also provides a new insight into the conversion between O_2^{2-} and $O^{-\cdot}$ radicals over metal oxides.

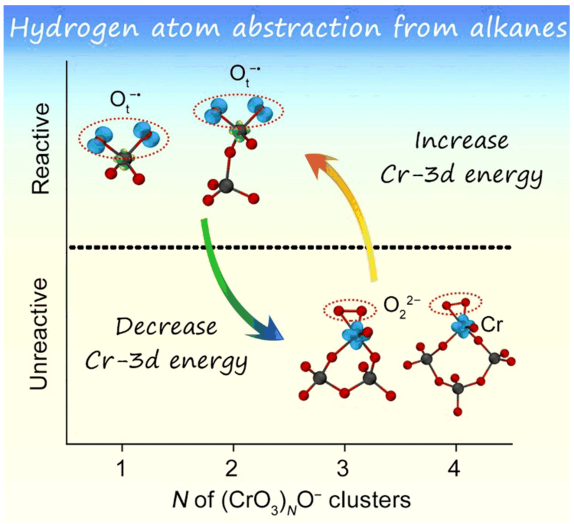

Key words: Reactive oxygen species, Alkane activation, Chromium oxide cluster, Mass spectrometry, Density functional theory calculation

I. INTRODUCTION

Alkanes originating from biogenic and fossil sources represent important raw materials in the chemical industry [1, 2]. It is extremely challenging to activate the C−H bonds under mild conditions in contemporary catalysis due to the inherent thermodynamic stability and kinetic inertness of alkanes [3−7]. Metal

†Part of the special topic for "the Chinese Chemical Society's 17th National Chemical Dynamics Symposium"
*Author to whom correspondence should be addressed. E-mail: chemzyx@iccas.ac.cn

oxides are extensively used as both catalysts and catalytic support materials for alkane conversion [7−10]. The catalytic role of metal oxide surfaces lies in their ability to form and provide oxygen in activated states. Reactive oxygen species (ROS) such as $O_2^{-\cdot}$ (superoxide radicals) [11−14], O_2^{2-} (peroxide species) [15, 16], and $O^{-\cdot}$ (oxygen-centered radicals) [17−20] that can be formed during the dissociation of molecular oxygen on the metal oxide surfaces via the general scheme of $O_2 \rightarrow O_2^{-\cdot} \rightarrow O_2^{2-} \rightarrow 2O^{-\cdot} \rightarrow 2O^{2-}$ (lattice oxygen) are considered as key intermediates for C−H activation. The $O^{-\cdot}$ radicals could be reactive to initiate hydrogen atom transfer (HAT) from alkanes, which was emphasized as a crucial step for the oxidative coupling of lower alkanes to higher hydrocarbons [10, 21−24]. By contrast, the $O_2^{-\cdot}$ and O_2^{2-} species were proposed to be much less reactive than $O^{-\cdot}$ radicals [17]. It is essential to discover factors that can manipulate the selective generation of $O^{-\cdot}$ radicals rather than $O_2^{-\cdot}$ radicals and O_2^{2-} species on metal oxides. However, it is difficult to differentiate the local active sites with different structures of metal oxides due to the complexity of condensed phase systems.

Investigation on the atomically precise metal oxide clusters in gas phase provides a distinctive approach to generalize the structure-activity relationship of metal oxides with different compositions and sizes [25−30]. Previous investigations found that the metal oxide clusters ($M_xO_y^q$) featuring with $\Delta \equiv 2y+q-nx=1$ usually contain $O^{-\cdot}$ radical sites [31], in which n is the highest oxidation state of the metal M and q is the charge number of the clusters. The 3d−5d metals located on the bottom-left side of the V-Mo-Re diagonal line in the periodic table are classified as metals of which the $M_xO_y^q$ (Δ=1) clusters contain $O^{-\cdot}$ radicals [31]. For example, the Δ=1 clusters of $(Sc_2O_3)_{1-22}^+$ [32], $(TiO_2)_{1-5}^+$ [33, 34], $(V_2O_5)_{1-11}^+$ [35, 36], $(Nb_2O_5)_{1-14}^+$ [37], $(Sc_2O_3)_{1-18}^-$ [38], $(V_2O_5)_{1-31}O^-$ [39, 40], and $(MoO_3)_{1-6}O^-$ [41] have been characterized to possess $O^{-\cdot}$ radical sites and can abstract a hydrogen atom from methane or other low-carbon alkanes. By contrast, the theoretical study about the oxide clusters of transition metals on the up-right side of the V-Mo-Re diagonal line predicted that the $Cr_xO_y^q$ clusters with Δ=1 (except CrO_4^-) do not contain $O^{-\cdot}$ radical sites [31], but there is no decisive experimental evidence to support the proposal.

In this context, the reactions of chromium oxide cluster anions $(CrO_3)_{1-4}O^-$ (Δ=1) towards C_1-C_4 alkanes have been experimentally investigated by utilizing our newly-developed ship-lock type reactor, which can measure the cluster reactions with a low detection limit of 10^{-18} $cm^3 \cdot molecule^{-1} \cdot s^{-1}$. While the CrO_4^- and $Cr_2O_7^-$ clusters can abstract a hydrogen atom from ethane and methane, respectively, the $(CrO_3)_{3,4}O^-$ clusters are unreactive with n-butane within the detection limit. Such a dramatically size-dependent reactivity reveals that the active sites of the $(CrO_3)_{1,2}O^-$ and $(CrO_3)_{3,4}O^-$ clusters are entirely different. Further DFT calculations show that the active sites of the $(CrO_3)_{1,2}O^-$ clusters could be characterized as $O^{-\cdot}$ radicals, while the $(CrO_3)_{3,4}O^-$ clusters possess the less reactive ROS of O_2^{2-}, which could be attributed to lower Cr-3d orbital energies affected by less delocalized negative charge within larger clusters. It is noteworthy that supported chromium oxide systems are active catalysts in a number of hydrocarbon reactions such as polymerization, dehydrogenation, and dehydrocyclization [42, 43].

II. METHODS

A. Experimental methods

The negatively charged chromium oxide clusters ($Cr_xO_y^-$) were generated by using a laser ablation method. A pulsed 532 nm laser (second harmonic of Nd^{3+}:YAG) with an energy of about 5−8 mJ and a repetition rate of 10 Hz was focused onto a chromium disk, the process of which could produce chromium metal plasma that reacted with 1%−5%O_2/He to form $Cr_xO_y^-$ cluster ions with different sizes and compositions. The clusters of interest $(CrO_3)_{1-4}O^-$ were mass-selected by using a quadrupole mass filter (QMF) and then entered into the ship-lock type reactor (SLTR). After the ions were thermalized by collisions with a pulse of He gas (about 2 Pa) for about 20 ms, two separate electromagnet valves were triggered to close the inlet and the outlet of the SLTR for a gas-tight condition. A pulse of reactant gas including C_1-C_4 alkanes and their deuterated compounds (up to around 100 Pa) except for C_2D_6 was then injected into the SLTR and interacted with the cluster ions. After reacting for about 100 ms or 700 ms, the valves were moved to open the inlet and outlet of the SLTR to expel the high-pressure reactant gas until the pressure was low enough to eject the ions from the SLTR. The ions were then guided by

DOI:10.1063/1674-0068/cjcp2303027

a hexapole system to enter into a reflectron time-of-flight mass spectrometer (Re-TOF-MS). The details for running the Re-TOF-MS, QMF, and the SLTR can be found in our previous work [44].

The rate constants (k_1) of the pseudo-first-order reactions between $(CrO_3)_{1-4}O^-$ clusters and alkanes were evaluated by the following equation:

$$I_R = \exp(-\rho k_1 t_R) \quad (1)$$

where I_R is the relative intensity of the reactant cluster ions, t_R is the reaction time, and ρ is the molecular density of alkanes that can be calculated by ρ=$P/(k_BT)$, in which P is the effective pressure of alkanes [44], k_B is the Boltzmann constant, and T is the temperature (298 K). The systematic deviations of t_R (±3%), T (±2%), P (±20%), and the uncertainty of I_R determined during fitting the k_1 values by Eq.(1) have been considered to calculate the errors of k_1 values. For kinetic isotope effect (KIE) values, both the systematic deviations of t_R (±3%) and T (±2%) can be neglected, thus, only the uncertainties of I_R and P (±20%) contribute to the errors of KIE values [45].

B. Computational methods

Density functional theory (DFT) calculations using Gaussian 16 program [46] were carried out to investigate the structures of reactant clusters $(CrO_3)_{1-4}O^-$ and the reaction mechanisms of $(CrO_3)_{1,2}O^-$ with CH_4. Two different functionals of B3LYP [47−49] and TPSS [50] were tested (Table SI in Supplementary materials, SM) and adopted to inspect the ground state structures of $(CrO_3)_{1-4}O^-$. The TZVP basis set [51] was used for all the atoms. The isomeric structures of CrO_4^- and $Cr_2O_7^-$ were obtained from the literatures [31, 52, 53]. A Fortran code based on a genetic algorithm [54] was used to search the global minimum structures of $(CrO_3)_{3,4}O^-$. More than 500 structures for $(CrO_3)_{3,4}O^-$ were generated with coarse thresholds, among which more than 10 low-lying energy isomers were reoptimized with strict thresholds. The lowest-lying optimized structures were considered as the isomers reacting with alkanes in the experiment. The reaction mechanism calculations involved geometry optimization of reaction intermediates (Is) and transition states (TSs) through which the Is transfer to each other. The initial structures of Is and TSs along the reaction pathways were obtained by performing the relaxed potential energy surface scans. Vibrational frequency calculations were conducted to check that the Is and TSs have zero and only one imaginary frequency, respectively. Each TS connecting two appropriate local minima was confirmed through intrinsic reaction coordinate calculations [55, 56]. The energies with zero-point vibration corrections (ΔH_0)and in unit of eV are reported in this work [45]. Natural charge analysis was calculated by NBO 5.9 [57].

The Rice-Ramsperger-Kassel-Marcus (RRKM) theory and RRKM-based variational transition-state theory (VTST) [58] were used to calculate the rate of traversing transition states and CH_4 desorption from adsorption complexes, respectively. For these calculations, the energy (E) of the initially formed adsorption complexes and the energy barrier ($E^{\neq}$) were needed. The E value included the vibrational energies (E_{vib}) of $Cr_xO_y^-$ and CH_4, the center-of-mass kinetic energy (E_k), and the binding energy (E_b) between $Cr_xO_y^-$ and CH_4. The values of E_{vib} and E_b were determined by the DFT calculations and E_k=$\mu v^2/2$, in which μ is the reduced mass and v is the velocity (∼550 m/s) [59]. The densities and the numbers of states required for RRKM and VTST calculations were obtained by the direct count method [60] with the DFT calculated vibrational frequencies under the approximation of harmonic vibrations.

Graphical structures are presented by using Visual Molecular Dynamics (VMD) [61]. All spin density distributions, orbitals, and surface electrostatic potentials were plotted by using Multiwfn [62] and VMD.

III. RESULTS AND DISCUSSION

A. Reactivity of $(CrO_3)_{1-4}O^-$ clusters

The TOF mass spectra for the reactions of mass-selected cluster anions $(CrO_3)_{1-4}O^-$ with n-C_4H_{10} at 298 K are plotted in FIG. 1. Upon the interaction of CrO_4^- with 0.93 Pa n-C_4H_{10} for about 100 ms (FIG. 1(a2)), the product peak assigned as CrO_4H^- becomes more intense relative to the background signal generated from the reaction with water impurity (FIG. 1(a1)), suggesting the occurrence of hydrogen atom abstraction (HAA) from n-C_4H_{10} to produce neutral $C_4H_9^{\cdot}$ radicals. Such a reaction channel also prevails in the reaction of $Cr_2O_7^-$ with n-C_4H_{10}. Moreover, the product ions of $Cr_2O_7H^-$ generated under a lower n-C_4H_{10} gas pressure of 0.10 Pa (FIG. 1(b2)) have a similar abundance to CrO_4H^- produced in

DOI:10.1063/1674-0068/cjcp2303027

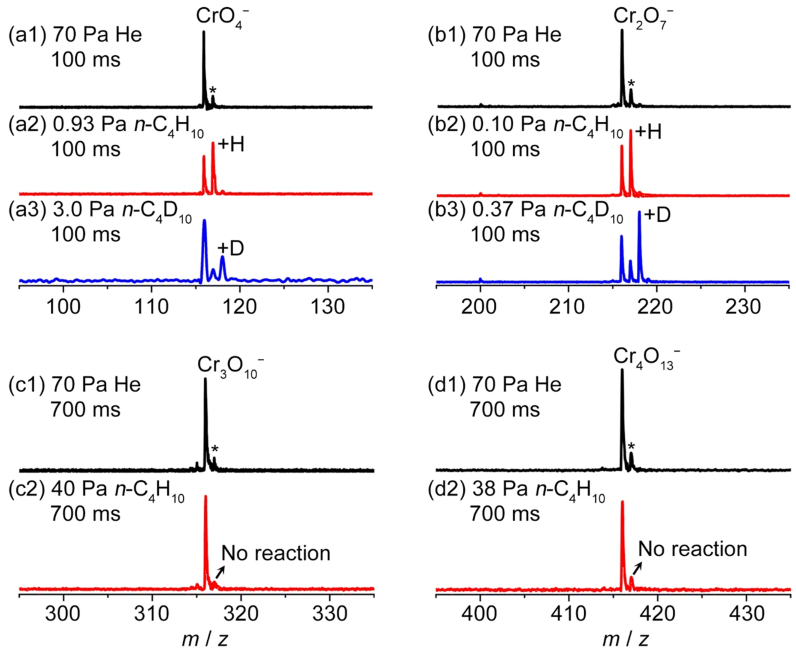

FIG. 1 TOF mass spectra for the reactions of (a, b) mass-selected $(CrO_3)_{1,2}O^-$ with *n*-C_4H_{10}/*n*-C_4D_{10} and (c, d) $(CrO_3)_{3,4}O^-$ with *n*-C_4H_{10}. The pressure of reactant gases and the reaction time are shown. The $Cr_xO_yX^-$ (X=H, D) species are labeled as +X. The peaks marked with asterisks are originated from the reactions with water impurities.

the reaction of CrO_4^- with a higher pressure of *n*-C_4H_{10}, indicating that $Cr_2O_7^-$ is more reactive than CrO_4^-. The identification of evident deuterium atom abstraction (DAA) products $(CrO_3)_{1,2}OD^-$ in the reactions of $(CrO_3)_{1,2}O^-$ with *n*-C_4D_{10} (FIG. 1 (a3) and (b3)) confirms the HAA reaction channel and also supports their relative activity. Differently, the reactions with much higher *n*-C_4H_{10} gas pressures (40 and 38 Pa) for a longer reaction time (700 ms) reveal that both $Cr_3O_{10}^-$ and $Cr_4O_{13}^-$ clusters are unreactive towards *n*-C_4H_{10} (FIG. 1 (c2) and (d2)). The experiments thus indicate a significant size-dependent reactivity of the $(CrO_3)_{1-4}O^-$ clusters in the order of $(CrO_3)_2O^- > (CrO_3)O^- >> (CrO_3)_{3,4}O^-$.

In addition to the activation of *n*-C_4H_{10}, the additional experiments demonstrate that the reactive $(CrO_3)_{1,2}O^-$ clusters could also abstract an H atom from C_2H_6 (7.5 and 4.5 Pa) and C_3H_8 (4.4 and 0.34 Pa) under a reaction time of 100 ms (FIG. 2 (a2, a3) and (b2, b3)). The HAA product $Cr_2O_7H^-$ was even observed in the reaction of $Cr_2O_7^-$ with the most inert alkane, CH_4, under the conditions of a CH_4 gas pressure of 75 Pa and a reaction time of 700 ms (FIG. 2(c2)), which was confirmed by the characterization of DAA product $Cr_2O_7D^-$ in the reaction of $Cr_2O_7^-$ with 142 Pa CD_4 (FIG. 2(c3)). The reaction of CrO_4^- with CH_4 has also been tested, however, it is difficult to observe the product due to the strong scattering of CrO_4^- ions with small mass by the high pressure (*e.g.*, 10 Pa) CH_4 gas pulsed into the reactor. The experimentally observed reaction channels can be summarized as follows:

$$(CrO_3)O^- + C_mH_{2m+2} \rightarrow (CrO_3)OH^- + C_mH_{2m+1}^{\cdot}, \quad m = 2-4 \tag{2}$$

$$(CrO_3)_2O^- + C_mH_{2m+2} \rightarrow (CrO_3)_2OH^- + C_mH_{2m+1}^{\cdot}, \quad m = 1-4 \tag{3}$$

$$(CrO_3)_{3,4}O^- + n\text{-}C_4H_{10} \rightarrow \text{no reaction} \tag{4}$$

Note that an evident peak assigned as $Cr_2O_6^-$ also appears in the reactions of $Cr_2O_7^-$ with CH_4 and CD_4, which is supposed as collision induced dissociation (CID) product confirmed by replacing CH_4 with

DOI:10.1063/1674-0068/cjcp2303027

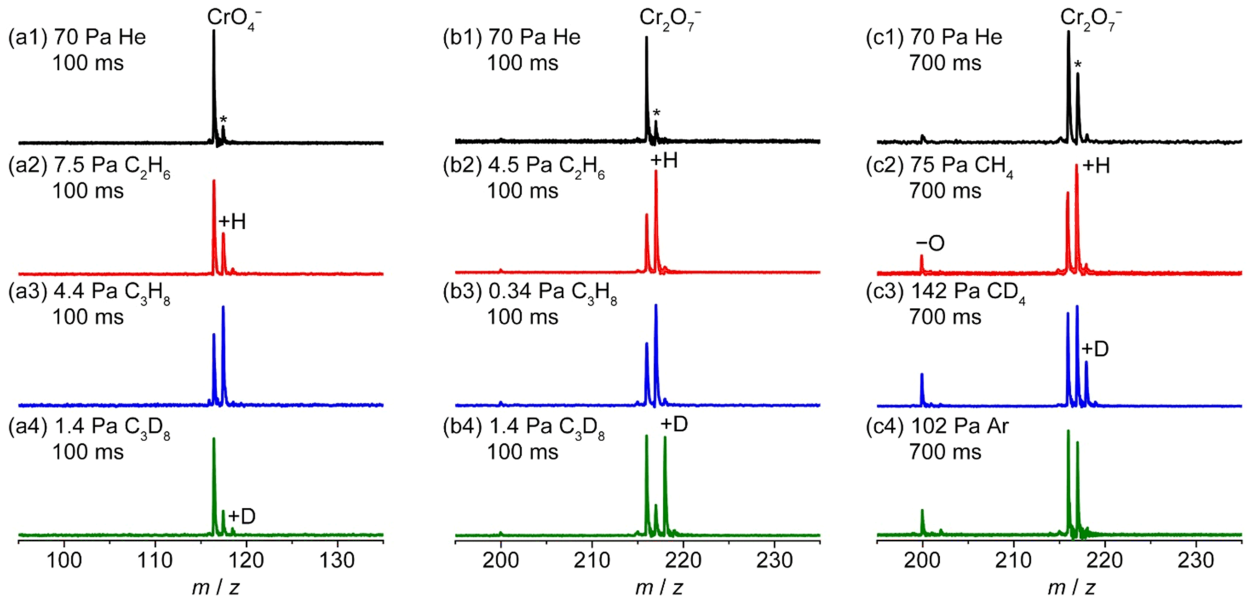

FIG. 2 TOF mass spectra for the reactions of (a) mass-selected CrO_4^- with C_2H_6, C_3H_8, and C_3D_8, and (b, c) $Cr_2O_7^-$ with C_2H_6, C_3H_8, C_3D_8, CH_4, CD_4, and Ar. The pressure of reactant gases and the reaction time are shown. The $Cr_xO_yX^-$ (X=H, D) species are labeled as +X. The peaks marked with asterisks are originated from the reactions with water impurities.

Ar as the reactant gas (FIG. 2(c4)).

Kinetic analysis of the depletion of $(CrO_3)_{1,2}O^-$ and the formation of corresponding HAA products as a function of alkane pressure was performed to quantify the rate constants (k_1) of the pseudo-first-order HAA reactions (FIG. S1 in SM). As shown in Table I, the k_1 value for the reaction of CrO_4^- with n-C_4H_{10} is determined as 3.8×10^{-14} cm^3·molecule^{-1}·s^{-1}, which is lower than that of the reaction between $Cr_2O_7^-$ and n-C_4H_{10} (2.6×10^{-13} cm^3·molecule^{-1}·s^{-1}). Such a reactivity difference between CrO_4^- and $Cr_2O_7^-$ is also observed in the reactions with C_2H_6 and C_3H_8 (Table I). The k_1 value for the reaction of $Cr_2O_7^-$ with CH_4 is evaluated as 3.7×10^{-17} cm^3·molecule^{-1}·s^{-1}. The kinetic isotope effects (KIE) for the reactions of the CrO_4^- and $Cr_2O_7^-$ clusters with n-C_4H_{10} and C_3H_8 are determined as 4.4−9.2 and 2.8−3.6, respectively (Table I and FIG. S2 in SM). The high KIE values indicate that the C−H bond activation corresponds to the rate-limiting step. It is noteworthy that the KIE value for CH_4 activation by $Cr_2O_7^-$ is evaluated as 2.5, which is lower than those of C_3H_8 and n-C_4H_{10} activation. Such a result may originate from the underestimation of $k_1(Cr_2O_7^-+CH_4)$ caused by the interference of intense background signal with the same m/z of $Cr_2O_7H^-$ that is generated from the reaction with water impurity for a long reaction time (FIG. 2(c1)).

B. Structural features of $(CrO_3)_{1-4}O^-$ clusters and reaction energetics

The DFT calculations have been performed to obtain the structural characteristics of the $(CrO_3)_{1-4}O^-$ clusters (FIG. S3 in SM). FIG. 3 presents two low-lying isomers possessing $O^{-\cdot}$ radicals or O_2^{2-} species (with bond lengths of 143−146 pm) for each $(CrO_3)_{1-4}O^-$ cluster. All of the structures are in doublet electronic states. Both B3LYP and TPSS levels predict that the lowest-lying isomer of CrO_4^- (IS1) has all four O atoms terminally (O_t) bonded with Cr atom and the unpaired spin density (UPSD) is delocalized on two O_t with the same value of 0.66 μ_B. The isomer IS2 with an O_2^{2-} unit is energetically higher than IS1 by 0.58−0.95 eV. The determinant of IS1 as the ground state structure of CrO_4^- was further supported by the photoelectron spectroscopy (PES) in literature [53]. Thus, the active site of CrO_4^- is delocalized $O^{-\cdot}$ radicals, in agreement with the HAA reactivity of CrO_4^- towards C_2−C_4 alkanes observed experimentally. For $Cr_2O_7^-$ cluster, the isomer IS4 possessing an O_2^{2-} unit was predicted as the lowest-lying isomer at B3LYP level in the previous computational study [31], while TPSS predicted IS3 as the lowest-lying isomer, the structure of which has two $Cr(O_t)_3$ units connected by a bridge-bonded O atom (O_b) and the UPSDs are delocalized over two

DOI:10.1063/1674-0068/cjcp2303027

TABLE I Experimentally determined absolute rate constants (k_1, with pseudo-first-order kinetic approximation) and kinetic isotopic effect (KIE=$k_{1,C_nH_{2n+2}}/k_{1,C_nD_{2n+2}}$) for HAA reactions of $(CrO_3)_{1,2}O^-$ with alkanes at 298 K.

Cluster	k_1/(cm^3·molecule^{-1}·s^{-1})				KIE[a]		
	CH_4	C_2H_6	C_3H_8	n-C_4H_{10}	CH_4[b]	C_3H_8	n-C_4H_{10}
CrO_4^-		$(1.1\pm0.4)\times10^{-15}$	$(1.1\pm0.2)\times10^{-14}$	$(3.8\pm0.8)\times10^{-14}$		9.2±3.8	4.4±0.4
$Cr_2O_7^-$	$(3.7\pm1.7)\times10^{-17}$	$(6.4\pm1.3)\times10^{-15}$	$(6.8\pm1.4)\times10^{-14}$	$(2.6\pm0.5)\times10^{-13}$	2.5±1.4	3.6±1.0	2.8±0.8

[a] The KIE values for the reactions with ethane were not measured due to the impurity of C_2D_6 gas preserved in our laboratory.
[b] The lower KIE value for the reaction of $Cr_2O_7^-$ with methane than propane and n-butane may originate from the underestimation of $k_1(Cr_2O_7^-+CH_4)$ caused by the interference of intense background signal with the same m/z of $Cr_2O_7H^-$ that was generated from the reaction with water impurity for a long reaction time (FIG. 2(c1)).

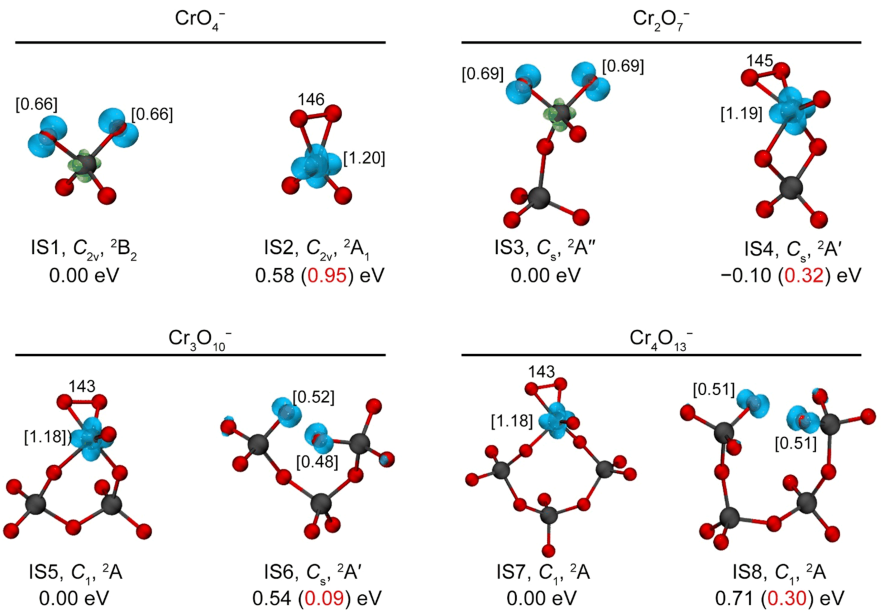

FIG. 3 DFT calculated the low-lying isomers of $(CrO_3)_{1-4}O^-$. Superscripts denote spin multiplicities. The symmetry, electronic states, and relative energies of the isomers calculated by B3LYP/TZVP and TPSS/TZVP (in parentheses) levels are listed below each structure. The UPSD distributions at B3LYP level are shown and the values are given in brackets. Some critical bond lengths at B3LYP level are given in pm.

O_t atoms (with the same value of 0.69 μ_B) that are located on one of the $Cr(O_t)_3$ units. The vertical detachment energies (VDEs) of IS3 and IS4 have been calculated and the simulated density of states (DOS) spectra were compared with the photoelectron spectroscopy (PES) of $Cr_2O_7^-$ reported by Wang *et al.* [63] (FIG. S4 and Table SII in SM). The VDE (5.81 eV) of IS3 is much closer to the experimental value (5.90 eV) than the VDE (5.22 eV) of IS4 predicted by B3LYP, moreover, the simulated DOS spectrum of IS3 matches well with the measured PES pattern. Despite that the deviations of TPSS computed VDEs of IS3 (5.43 eV) and IS4 (4.88 eV) from the experimental values are relatively large, only the simulated DOS spectrum of IS3 could be comparable to the experimental observation. Such a comparative study thus implies that IS3 is more likely to be the ground state structure of $Cr_2O_7^-$. The assignment of IS3 with the delocalized $O^{-\cdot}$ radicals as the lowest-lying isomer of $Cr_2O_7^-$ can be further supported by the ion mobility mass spectrometry conducted by Misaizu *et al.* [52], rationalizing the experimental identification of HAA from C_1-C_4 alkanes by $Cr_2O_7^-$ and the release of an O atom from $Cr_2O_7^-$ during the CID by Ar gas. With further increase of cluster size, the most stable structures of $Cr_3O_{10}^-$ and $Cr_4O_{13}^-$ evolve to the isomers with O_2^{2-} species (IS5 and IS7) rather than the isomers with $O^{-\cdot}$ radicals (IS6 and IS8) at both B3LYP and TPSS levels. The UPSD of each cluster is mainly localized on the Cr atom bonded to O_2^{2-} species with the same value of 1.18 μ_B. Such structural char-

DOI:10.1063/1674-0068/cjcp2303027

acteristics of $(CrO_3)_{3,4}O^-$ clarify their inferior activity due to the extremely low reactivity of O_2^{2-} species towards alkanes [17].

Mechanistic studies about the reaction paths of HAA from CH_4 by the ground states of CrO_4^- and $Cr_2O_7^-$ at B3LYP level demonstrate that Cr−$O_t^{-\cdot}$-mediated C−H activation undergoes the hydrogen-atom transfer mechanism (FIG. 4). For the reaction of CrO_4^- with CH_4, an encounter complex (I1) formed with a small binding energy of 0.05 eV encounters an overall positive barrier of 0.42 eV to cleave the C−H bond (TS1) and the generation of product $CH_3^\cdot$ (P1) is slightly endothermic with reaction enthalpy ($\Delta H_{0\,K}$) of 0.06 eV (FIG. 4(a)). On the contrary, the association complex formed by the reaction of $Cr_2O_7^-$ and CH_4 (I3) with a small binding energy of 0.01 eV experiences a lower positive barrier of 0.24 eV to break the C−H bond (TS2), moreover, the production of $CH_3^\cdot$ (P2) is exothermic by $\Delta H_{0\,K}$=−0.16 eV (FIG. 4(b)). The lower C−H activation barrier and more favorable thermodynamics for the reaction of $Cr_2O_7^-$ with CH_4 are consistent with the experimental result that the HAA product absent in the reaction system of CrO_4^- is observed in the reaction couple of $Cr_2O_7^-/CH_4$. It should be noted that the positive barrier (0.24 eV) for the reaction of $Cr_2O_7^-$ with CH_4 could be overcome by the total energy carried by I3 including the center-of-mass kinetic energy (E_k≈0.03 eV) and vibrational energies (E_{vib}=0.37 eV at T=298 K by DFT) of the separated reactants. The RRKM theory [58] calculations indicate that the rate of internal conversion (k_{int}) (I3→TS2→I4) is 7.0×10^2 s^{-1} and the rate of back dissociation (k_d) [I3→$Cr_2O_7^-$+CH_4] is 6.4×10^{11} s^{-1}. The k_{int} value is much smaller than k_d by about nine orders of magnitude, which is qualitatively in agreement with the low rate constant of 3.7×10^{-17} $cm^3\cdot molecule^{-1}\cdot s^{-1}$ determined in experiments. In addition, the potential energy surfaces for the reactions of $(CrO_3)_{1,2}O^-$ clusters with C_2H_6 have also been calculated (FIG. S5 in SM). The lower barrier invovled in C−H activation and higher exothermicity of $C_2H_5^\cdot$ production in the reaction couple $Cr_2O_7^-/C_2H_6$ also support the higher reactivity of $Cr_2O_7^-$ identified experimentally. On the contrary, the reaction barriers for n-C_4H_{10} activation by $Cr_3O_{10}^-$ and $Cr_4O_{13}^-$ clusters are as high as 1.28 eV (FIG. S6 in SM), in consistent with the inertness of $(CrO_3)_{3,4}O^-$ observed in experiments.

Previous investigations on the reactions between

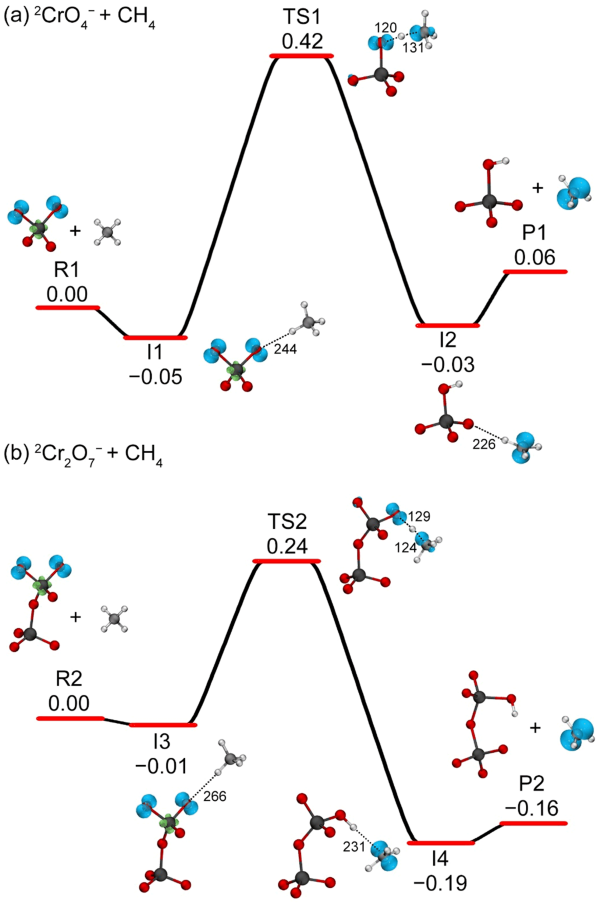

FIG. 4 B3LYP functional calculated potential energy profiles for the reactions of CrO_4^- (IS1, a) and $Cr_2O_7^-$ (IS3, b) with CH_4. The relative energies (ΔH_0, eV) of the reaction intermediates, transition states, and products with respect to the separated reactants are given. The UPSD distributions and some critical bond lengths (pm) are shown.

metal oxide clusters and alkanes proposed that the local charges [26, 64, 65] and UPSD distributions [26, 27, 66] around $O^{-\cdot}$ radicals function are key factors to tune the HAA reactivity of $O^{-\cdot}$ radicals. More positive (or less negative) local charges or higher UPSD values correspond to higher HAA reactivity. To clarify the different reactivity of CrO_4^- and $Cr_2O_7^-$ towards alkanes, the UPSD distributions and the local charges around $O^{-\cdot}$ radicals have been analyzed. While the UPSD values of the delocalized $O^{-\cdot}$ radicals are nearly identical (0.66 and 0.69 μ_B, FIG. 3), the local charges around $O^{-\cdot}$ radicals are very different. The local charges (Q_L) are defined as follows [64]:

$$Q_L \equiv Q(M) + \sum_{i=1}^{N} \frac{Q(O_i)}{f_i} \quad (5)$$

DOI:10.1063/1674-0068/cjcp2303027

in which $Q(\mathrm{M})$ and $Q(\mathrm{O}_i)$ are the charge from natural population analysis on the metal atom (M) and the ith O atom that is directly bonded with M and f_i-fold coordinated in the cluster, respectively. For the CrO_4^- cluster, the simple geometrical structure of one Cr atom center bonded with four O_t atoms leads to a local charge value of −1 e around $O^{-\cdot}$ radicals according to Eq.(5). However, the unit negative charge is delocalized on two CrO_y units in the $Cr_2O_7^-$ cluster, resulting in the less negative local charge around $O^{-\cdot}$ radicals with a value of −0.33 e, which could provide a larger driving force to pull the electrons from alkanes and account for the higher HAA reactivity of $Cr_2O_7^-$.

C. Mechanism for the evolution of active sites from O_2^{2-} species to $O^{-\cdot}$ radicals along cluster size

The O_2^{2-} species can be considered as intermediates to generate $O^{-\cdot}$ radicals during oxygen dissociation on metal oxide surfaces [67]. Rushiti and Hättig previously reported that the dioxygen species dissociating into monoatomic ROS on the (001) surfaces of $CoFe_2O_4$ was identified as one electron process, in which the electron was provided from metal centers [68]. However, the factors that facilitate the reduction of O_2^{2-} species to $O^{-\cdot}$ radicals remain ambiguous due to the complexity of the condensed phase system. Understanding the molecular-level mechanism for the transition of the active sites from O_2^{2-} species to $O^{-\cdot}$ radicals along the $(CrO_3)_NO^-$ cluster size is helpful for providing insights into controlling the isomerization of ROS in practical materials.

As discussed above, the UPSD distributions of $(CrO_3)_NO^-$ (N=1−4) isomers with $O_t^{-\cdot}$ radical and O_2^{2-} sites are mainly localized on $O_t^{-\cdot}$ radicals and Cr metal center, respectively (FIG. 3), which suggests the occurrence of electron transfer from Cr atom to ROS sites during the isomerization processes. The analysis on molecular orbitals of $(CrO_3)_{1-4}O^-$ with O_2^{2-} sites shows that the energy of singly occupied molecular orbitals (SOMOs), which are mainly composed of 3d orbitals of Cr bonded to O_2^{2-}, increases as the cluster size decreases (FIG. 5(a)). Such a result indicates that the Cr atom progressively becomes easier to donate the unpaired electron to O_2^{2-} from N=4 to N=1, and thus the O_2^{2-} species in smaller $(CrO_3)_NO^-$ clusters are more likely to be reduced, resulting in the generation of $O_t^{-\cdot}$ radicals.

The net negative charge of the $(CrO_3)_{1-4}O^-$ cluster is generally delocalized on multiple CrO_y units. As shown in FIG. 5(a), the charges around the $(O_b)_2CrO_t(O-O)$ unit become less negative as the residual cluster skeleton grows and possesses more negative charges, which could lower the Cr-3d orbital energy. The electrostatic potentials of the $(CrO_3)_{1-4}O^-$ clusters also reveal that the charge around Cr metal center becomes less negative as N increases (FIG. 5(b)), further supporting the variation of Cr-3d orbital energy with respect to the cluster size. Therefore, it could be concluded that the more negative charge environments leading to higher Cr-3d orbital energies are responsible for the more favorable generation of $O^{-\cdot}$ radicals in $(CrO_3)_{1,2}O^-$ clusters. It is noteworthy that chromia-based catalysts are highly reactive and selective in oxidative dehydrogenation (ODH) of isobutene [42, 69, 70]. Oxygen chemisorption experiment conducted by Sloczyński *et al.* [42] revealed that the rate of dissociative adsorption of oxygen (molecular oxygen→atomic oxygen) could account for the reaction rates of ODH of isobutane. The manipulation of Cr-3d orbital energies

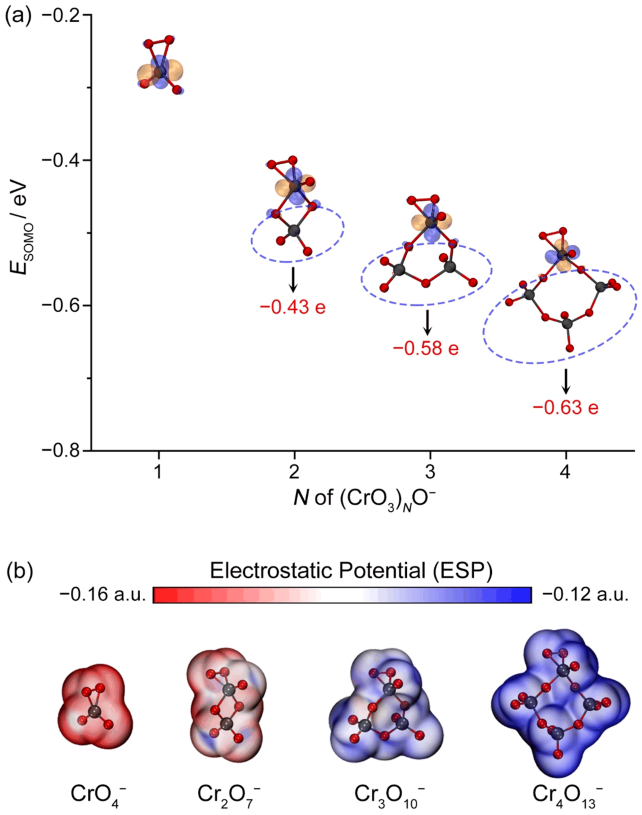

FIG. 5 (a) DFT calculated SOMO energy levels of $(CrO_3)_{1-4}O^-$ clusters. The sums of natural charges for the atoms encircled are given. (b) Electrostatic potential maps for $(CrO_3)_{1-4}O^-$ clusters.

DOI:10.1063/1674-0068/cjcp2303027

by tuning the size of chromium oxide clusters to facilitate the formation of atomic oxygen species (*e.g.*, $O^{-\cdot}$ radicals) discovered in this study may shed light into the activity of chromia-based catalysts in condensed systems.

IV. CONCLUSION

In summary, the abstraction of a hydrogen atom from C_1-C_4 alkanes by chromium oxide cluster anions CrO_4^- and $Cr_2O_7^-$ has been experimentally characterized at 298 K, and the rate constants were quantified in the orders of magnitude of $10^{-13}-10^{-16}$ $cm^3 \cdot molecule^{-1} \cdot s^{-1}$. However, the larger clusters $Cr_3O_{10}^-$ and $Cr_4O_{13}^-$ were inert even towards n-C_4H_{10} within the detection limit (1×10^{-18} $cm^3 \cdot molecule^{-1} \cdot s^{-1}$) of our apparatus. Density functional theory calculations revealed that the reactive clusters CrO_4^- and $Cr_2O_7^-$ possess the active sites of delocalized $O^{-\cdot}$ radicals, while the unpaired electron is localized on Cr atoms in both $Cr_3O_{10}^-$ and $Cr_4O_{13}^-$ clusters, leading to the formation of unreactive O_2^{2-} sites. Because of the lower Cr-3d orbital energy caused by the less negative charge environment as the cluster skeleton grows, the unpaired electron localized on Cr atom becomes more difficult to reduce O_2^{2-} unit. This study not only characterizes Cr-$O^{-\cdot}$-mediated alkane activation in the gas-phase cluster chemistry, but also provides a regulation rule for the selective conversion of sluggish O_2^{2-} species into reactive $O^{-\cdot}$ radicals over metal oxides.

Supplementary material: Additional experimental results about kinetic analysis for the reactions of $(CrO_3)_{1,2}O^-$ with C_1-C_4 alkanes and theoretical results about structures of $(CrO_3)_{1-4}O^-$ clusters as well as reaction pathways are available.

V. ACKNOWLEDGMENTS

This work was supported by the National Natural Science Foundation of China (No.92161205 and No.92061115), and the Youth Innovation Promotion Association CAS (No.2018041).

[1] G. A. Olah and Á. Molnár, *General Aspects. Hydrocarbon Chemistry*, 1 (2003).
[2] Y. Wang, P. Hu, J. Yang, and Y. A. Zhu, and D. Chen, Chem. Soc. Rev. **50**, 4299 (2021).
[3] R. A. Periana, D. J. Taube, S. Gamble, H. Taube, T. Satoh, and H. Fujii, Science **280**, 560 (1998).
[4] C. Coperet, Chem. Rev. **110**, 656 (2010).
[5] A. A. Latimer, A. R. Kulkarni, H. Aljama, J. H. Montoya, J. S. Yoo, C. Tsai, F. Abild-Pedersen, F. Studt, and J. K. Nørskov, Nat. Mater. **16**, 225 (2017).
[6] J. L. Lee, D. L. Ross, S. K. Barman, J. W. Ziller, and A. S. Borovik, Inorg. Chem. **60**, 13759 (2021).
[7] R. Martin, M. Kim, A. Asthagiri, and J. F. Weaver, ACS Catal. **11**, 4682 (2021).
[8] J. F. Weaver, C. Hakanoglu, A. Antony, and A. Asthagiri, Chem. Soc. Rev. **43**, 7536 (2014).
[9] S. D. Senanayake, J. A. Rodriguez, and J. F. Weaver, Acc. Chem. Res. **53**, 1488 (2020).
[10] X. Li, C. Pei, and J. Gong, Chem **7**, 1755 (2021).
[11] M. Hayyan, M. A. Hashim, and I. M. AlNashef, Chem. Rev. **116**, 3029 (2016).
[12] K. i. Ishibashi, Y. Nosaka, K. Hashimoto, and A. Fujishima, J. Phys. Chem. B **102**, 2117 (1998).
[13] J. H. Lunsford, Catal. Rev. **8**, 135 (1974).
[14] T. Tachikawa and T. Majima, Langmuir **25**, 7791 (2009).
[15] M. Che and A. J. Tench, *Characterization and Reactivity of Molecular Oxygen Species on Oxide Surfaces*. In: D. D. Eley, H. Pines, and P. B. Weisz, Eds. *Advances in Catalysis*, San Diego, CA: Academic Press, 1 (1983).
[16] O. C. Williams and C. Sievers, Appl. Catal. A: Gen. **614**, 118057 (2021).
[17] G. I. Panov, K. A. Dubkov, and E. V. Starokon, Catal. Today **117**, 148 (2006).
[18] A. M. Volodin, V. I. Avdeev, S. E. Malykhin, and A. F. Bedilo, Res. Chem. Intermed. **43**, 1047 (2017).
[19] X. Meng, X. Cui, N. P. Rajan, L. Yu, D. Deng, and X. Bao, Chem **5**, 2296 (2019).
[20] G. I. Panov, E. V. Starokon, D. P. Ivanov, L. V. Pirutko, and A. S. Kharitonov, Catal. Rev. **63**, 597 (2021).
[21] S. Arndt, G. Laugel, S. Levchenko, R. Horn, M. Baerns, M. Scheffler, R. Schlögl, and R. Schomäcker, Catal. Rev. **53**, 424 (2011).
[22] J. H. Lunsford, Catal. Today **63**, 165 (2000).
[23] R. Schłgl, Angew. Chem. Int. Ed. **54**, 3465 (2015).
[24] J. Sun, J. W. Thybaut, and G. B. Marin, Catal. Today **137**, 90 (2008).
[25] R. A. J. O'Hair and G. N. Khairallah, J. Cluster Sci. **15**, 331 (2004).
[26] X. L. Ding, X. N. Wu, Y. X. Zhao, and S. G. He, Acc. Chem. Res. **45**, 382 (2012).
[27] N. Dietl, M. Schlangen, and H. Schwarz, Angew. Chem. Int. Ed. **51**, 5544 (2012).
[28] S. M. Lang and T. M. Bernhardt, Phys. Chem. Chem. Phys. **14**, 9255 (2012).
[29] N. Levin, J. Lengyel, J. F. Eckhard, M. Tschurl, and U. Heiz, J. Am. Chem. Soc. **142**, 5862 (2020).
[30] C. A. Gaggioli, J. Sauer, and L. Gagliardi, J. Am. Chem. Soc. **141**, 14603 (2019).

DOI:10.1063/1674-0068/cjcp2303027

[31] Y. X. Zhao, X. L. Ding, Y. P. Ma, Z. C. Wang, and S. G. He, Theor. Chem. Acc. **127**, 449 (2010).
[32] X. N. Wu, B. Xu, J. H. Meng, and S. G. He, Int. J. Mass spectrom. **310**, 57 (2012).
[33] Y. X. Zhao, X. N. Wu, Z. C. Wang, S. G. He, and X. L. Ding, Chem. Commun. **46**, 1736 (2010).
[34] J. N. Harvey, M. Diefenbach, D. Schröder, and H. Schwarz, Int. J. Mass spectrom. **182/183**, 85 (1999).
[35] S. Feyel, J. Döbler, D. Schröder, J. Sauer, and H. Schwarz, Angew. Chem. Int. Ed. **45**, 4681 (2006).
[36] X. N. Wu, X. L. Ding, Z. Y. Li, Y. X. Zhao, and S. G. He, J. Phys. Chem. C **118**, 24062 (2014).
[37] X. L. Ding, D. Wang, X. N. Wu, Z. Y. Li, Y. X. Zhao, and S. G. He, J. Chem. Phys. **143**, 124312 (2015).
[38] L. H. Tian, J. H. Meng, X. N. Wu, Y. X. Zhao, X. L. Ding, S. G. He, and T. M. Ma, Chem. Eur. J. **20**, 1167 (2014).
[39] M. Q. Zhang, Y. X. Zhao, Q. Y. Liu, X. N. Li, and S. G. He, J. Am. Chem. Soc. **139**, 342 (2017).
[40] G. P. Wei, Y. X. Zhao, and S. G. He, J. Chem. Phys. **157**, 154304 (2022).
[41] M. Ruan, Y. X. Zhao, M. Q. Zhang, and S. G. He, Chem. Eur. J. **28**, e202103321 (2022).
[42] J. Słoczyński, B. Grzybowska, R. Grabowski, A. Kozłowska, and K. Wcisło, Phys. Chem. Chem. Phys. **1**, 333 (1999).
[43] M. P. McDaniel, *Supported Chromium Catalysts for Ethylene Polymerization*. In: D. D. Eley, H. Pines, and P. B. Weisz Eds., *Advances in Catalysis*, San Diego, CA: Academic Press, 47 (1985).
[44] G. P. Wei, Q. Y. Liu, Y. Ren, and S. G. He, Rev. Sci. Instrum. **92**, 104104 (2021).
[45] Y. K. Li, Z. Y. Li, Y. X. Zhao, Q. Y. Liu, J. H. Meng, and S. G. He, Chem. Eur. J. **22**, 1825 (2016).
[46] M. J. Frisch, G. W. Trucks, H. B. Schlegel, G. E. Scuseria, M. A. Robb, J. R. Cheeseman, G. Scalmani, V. Barone, G. A. Petersson, H. Nakatsuji, X. Li, M. Caricato, A. V. Marenich, J. Bloino, B. G. Janesko, R. Gomperts, B. Mennucci, H. P. Hratchian, J. V. Ortiz, A. F. Izmaylov, J. L. Sonnenberg, Williams, F. Ding, F. Lipparini, F. Egidi, J. Goings, B. Peng, A. Petrone, T. Henderson, D. Ranasinghe, V. G. Zakrzewski, J. Gao, N. Rega, G. Zheng, W. Liang, M. Hada, M. Ehara, K. Toyota, R. Fukuda, J. Hasegawa, M. Ishida, T. Nakajima, Y. Honda, O. Kitao, H. Nakai, T. Vreven, K. Throssell, J. A. Montgomery Jr., J. E. Peralta, F. Ogliaro, M. J. Bearpark, J. J. Heyd, E. N. Brothers, K. N. Kudin, V. N. Staroverov, T. A. Keith, R. Kobayashi, J. Normand, K. Raghavachari, A. P. Rendell, J. C. Burant, S. S. Iyengar, J. Tomasi, M. Cossi, J. M. Millam, M. Klene, C. Adamo, R. Cammi, J. W. Ochterski, R. L. Martin, K. Morokuma, O. Farkas, J. B. Foresman, and D. J. Fox, *Gaussian 16 Rev. C.01*, Wallingford, CT: Gaussian Inc., (2016).
[47] C. T. Lee, W. T. Yang, and R. G. Parr, Phys. Rev. B **37**, 785 (1988).
[48] A. D. Becke, Phys. Rev. A **38**, 3098 (1988).
[49] A. D. Becke, J. Chem. Phys. **98**, 5648 (1993).
[50] J. Tao, J. P. Perdew, V. N. Staroverov, and G. E. Scuseria, Phys. Rev. Lett. **91**, 146401 (2003).
[51] A. Schäfer, C. Huber, and R. Ahlrichs, J. Chem. Phys. **100**, 5829 (1994).
[52] R. Moriyama, R. Sato, M. Nakano, K. Ohshimo, and F. Misaizu, J. Phys. Chem. A **121**, 5605 (2017).
[53] G. L. Gutsev, P. Jena, H. J. Zhai, and L. S. Wang, J. Chem. Phys. **115**, 7935 (2001).
[54] X. L. Ding, Z. Y. Li, J. H. Meng, Y. X. Zhao, and S. G. He, J. Chem. Phys. **137**, 214311 (2012).
[55] C. Gonzalez and H. B. Schlegel, J. Chem. Phys. **90**, 2154 (1989).
[56] C. Gonzalez and H. B. Schlegel, J. Phys. Chem. **94**, 5523 (1990).
[57] E. D. Glendening, J. K. Badenhoop, A. E. Reed, J. E. Carpenter, J. A. Bohmann, C. M. Morales, and F. Weinhold, *NBO 5.9,* University of Wisconsin, Madison, WI: Theoretical Chemistry Institute, (2012).
[58] J. I. Steinfeld, J. S. Francisco, and W. L. Hase, *Chemical Kinetics and Dynamics*, Upper Saddle River, NJ: Prentice Hall, (1999).
[59] J. H. Meng, X. J. Deng, Z. Y. Li, S. G. He, and W. J. Zheng, Chem. Eur. J. **20**, 5580 (2014).
[60] T. Beyer and D. F. Swinehart, Commun. ACM **16**, 379 (1973).
[61] W. Humphrey, A. Dalke, and K. Schulten, J. Mol. Graphics **14**, 33 (1996).
[62] T. Lu and F. Chen, J. Comput. Chem. **33**, 580 (2012).
[63] H. J. Zhai, X. Huang, T. Waters, X. B. Wang, R. A. J. O'Hair, A. G. Wedd, and L. S. Wang, J. Phys. Chem. A **109**, 10512 (2005).
[64] Z. Y. Li, Y. X. Zhao, X. N. Wu, X. L. Ding, and S. G. He, Chem. Eur. J. **17**, 11728 (2011).
[65] Y. X. Zhao, X. N. Wu, J. B. Ma, S. G. He, and X. L. Ding, Phys. Chem. Chem. Phys. **13**, 1925 (2011).
[66] X. N. Wu, Y. X. Zhao, W. Xue, Z. C. Wang, S. G. He, and X. L. Ding, Phys. Chem. Chem. Phys. **12**, 3984 (2010).
[67] C. Li, K. Domen, K. Maruya, and T. Onishi, J. Am. Chem. Soc. **111**, 7683 (1989).
[68] A. Rushiti and C. Hattig, Chem. Eur. J. **27**, 17115 (2021).
[69] J. Słoczyński, B. Grzybowska, A. Koz-owska, K. Samson, R. Grabowski, A. Kotarba, and M. Hermanowska, Catal. Today **169**, 29 (2011).
[70] J. T. Grant, J. M. Venegas, W. P. McDermott, and I. Hermans, Chem. Rev. **118**, 2769 (2018).

DOI:10.1063/1674-0068/cjcp2303027